

Supplement of Geosci. Model Dev., 13, 2337–2354, 2020  
<https://doi.org/10.5194/gmd-13-2337-2020-supplement>  
© Author(s) 2020. This work is distributed under  
the Creative Commons Attribution 4.0 License.



*Supplement of*

**Development of a sequential tool, LMDZ-NEMO-med-V1, to conduct  
global-to-regional past climate simulation for the Mediterranean basin:  
an Early Holocene case study**

**Tristan Vadsaria et al.**

*Correspondence to:* Tristan Vadsaria (vadsaria@aori.u-tokyo.ac.jp, tristan.vadsaria@lsce.ipsl.fr)

The copyright of individual parts of the supplement might differ from the CC BY 4.0 License.

1  
2  
3  
4  
5  
6  
7  
8  
9  
10  
11  
12  
13  
14  
15  
16  
17  
18  
19  
20  
21  
22  
23  
24  
25  
26  
27  
28  
29  
30  
31  
32  
33

The supplementary material includes:

- **Supplementary text**

**Text S1:** LMDZ-NEMO-med, user manual

**Text S2:** Bias correction

**Text S2:** Comparison of model simulation outputs with reconstructed data for the whole Mediterranean basin

- **Supplementary figures**

**Fig. S1.** Runoff of the Nile River

**Fig. S2.** Model/reconstruction data comparison for SST

**Fig. S3.** Model/reconstruction data comparison for SSS

**Fig. S4.** Time series of IS over the Mediterranean Sea in HIST

**Fig. S5.** Time series of maximum ZOF in the eastern Mediterranean Sea in HIST

**Fig. S6.** Time series of IS over the Mediterranean Sea in PICTRL and EHOL

**Fig. S7.** Time series of maximum ZOF in the eastern Mediterranean Sea in PICTRL and EHOL

**Fig. S8.** Time series of SSS for the Mediterranean Sea in PICTRL and EHOL

- **Supplementary tables**

**Tab. S1.** Model-data comparison for continental precipitation

**Tab. S2.** Forcings and parameters used in both AGCM and ARCM

**Tab. S3.** Forcings used in the ORCM

## 34 **Text S1: LMDZ-NEMO-med, user manual**

35

36 This section is intended as a user manual to explain how to compile and run LMDZ-NEMO-med on a  
37 Linux system. It is not, however, a detailed description of the source code. Files relevant to the  
38 running of the pre-industrial control simulation presented in the article have been archived and made  
39 publicly available for downloading: <https://zenodo.org/record/3258410> (Vadsaria et al., 2019).

40

### 41 1 Atmospheric global model

42 LMDz4, used here in both the global and regional versions, is version 4 of the LMDZ model. It has the  
43 same major code structure and practical organization as what is consultable on the web page:  
44 [https://forge.ipsl.jussieu.fr/igcmg\\_doc/wiki/DocImodelBlmdz](https://forge.ipsl.jussieu.fr/igcmg_doc/wiki/DocImodelBlmdz)

45

#### 46 1.1 Compiling the model

47 The compiling environment is MODIPSL, a convention for code compilation when the code is  
48 distributed into different directories. The following directory should be consulted:

49 **“cd vadsaria\_et\_al\_model/LMDZ\_and\_NEMOMED8\_models/modipsl/util”**

50 Edit the **“AA\_make.gdef”**: the user should create a new entry to fit its computational architecture.  
51 Compiler options have been set up in this file and will be propagated to **“Makefile”** at different places.

52

53 It is recommended that all previous configurations be cleared by typing **“./clr\_make”**. A new  
54 configuration to match the right computer platform can then be created:

55 **“./ins\_make -t NAME\_OF\_YOUR\_ARCHITECTURE\_SYSTEM”**

56 Before code compilation, the library netcdf and a Fortran compiler need to be installed. FCM (Flexible  
57 Configuration Management: <https://metomi.github.io/fcm/doc/>), a tool developed by the UK Met  
58 Office to manage the dependence among different subroutines of a complex code is also required.  
59 Compiling options for FCM are stored under **“machine/arch.path”** and **“machine/arch.fcm”**. They need  
60 to be coherent with what stored under **“AA\_make.gdef”** and **“Makefile”**.

61 To compile the code, the following directory needs to be consulted:

62 **“cd vadsaria\_et\_al\_model/LMDZ\_and\_NEMOMED8\_models/modipsl/config/LMDZ”**

63 Then, with the help of **“Makefile”**, the following can be compiled:

64 **“gmake lmdz96x71global”**

65 where **“lmdz96x71global”** is a keyword defined in the **“AA\_make”** script allowing a configuration to  
66 be chosen.

67 If the compilation is successful, then the executable codes **“create\_etat0\_limit.e”**,  
68 **“make\_relax\_times.e”** and **“gcm.e”** are stocked at the following directory:

69 **“cd vadsaria\_et\_al\_model/LMDZ\_and\_NEMOMED8\_models/modipsl/modipsl/bin”**

70

71 1.2 Running the model

72

73 The first step is the creation of boundary conditions for the global atmospheric model. The supporting  
74 files needed for this step can be found in the following directory:

75 **“cd vadsaria\_et\_al\_model/files\_and\_boundary\_conditions\_for\_LMDZ\_global/start\_limit”**

76

77 A boundary condition file is already provided in this directory: **“limit\_picontrol\_debias.nc”**. It is  
78 based on a bias-corrected file for SST and SIC data (following the procedure described in the main  
79 article) derived from the IPSLCM5 model for the pre-industrial simulation. The procedure to generate  
80 this boundary condition file is the following:

81 - Prepare a netcdf file with SST and SIC bias-corrected data, interpolated on a  $1^\circ \times 1^\circ$  grid: **“CM5-  
82 piControl-pseudo\_amip\_1x1\_tos\_sic.3600-3699\_climato.after\_correction.nc”** (in the sub-  
83 directory **“/interpol”**, a code to generate a  $1^\circ \times 1^\circ$  **“AMIP”** grid is provided :  
84 **“interpol\_ipslcm5\_amip\_tos\_sic.F90”**)

85 - Create symbolic links:

86 **“ln -s CM5-piControl-pseudo\_amip\_1x1\_tos\_sic.3600-3699\_climato.after\_correction.nc  
87 amipbc\_sic\_1x1.nc”**

88 **“ln -s CM5-piControl-pseudo\_amip\_1x1\_tos\_sic.3600-3699\_climato.after\_correction.nc  
89 amipbc\_sst\_1x1.nc”**

90 - Move the file obtained from the previous compilation of the model to the current directory and  
91 execute:

92 **“./create\_etat0\_limit.e”**

93

94 This execution is based on a few **“.nc”** files containing information on topography, surface albedo, etc.  
95 It also takes relevant information from definition files of the model (**gcm.def**, **physic.def** and  
96 **orchidee.def**). It should create a **“limit.nc”** file.

97 After creating the initial states and boundary conditions, we are now ready to run the model with an  
98 example from the following directory

99 **“cd vadsaria\_et\_al\_model/files\_and\_boundary\_conditions\_for\_LMDZ\_global”**

100

101 The bash script **“launch\_picontrol\_run\_global\_type”** is an example of how to run the atmospheric  
102 global model. The script firstly organizes files for boundary conditions and initial state (all presented  
103 in the current directory), and then executes the model **“gcm.e”** to generate outputs. This script was  
104 initially created for use in the supercomputing centre TGCC. It contains some TGCC-specific  
105 instructions for the management of environmental variables, including the necessary pathways for the  
106 model’s preferences and allocation of computing resources. The script is executed with a time step of  
107 one month.

108

109 To start the execution of the model:

110 **./launch\_picontrol\_run\_global\_make 1**

111

112 “1” being the first month. It will create the **launch\_picontrol\_run\_global\_launcher** bash file. The  
113 user should then execute this file according to the actual operating system. If the script works, it will  
114 automatically generate the next iteration (the next month) until the maximum iteration is reached,  
115 denoted as the “**stop**” variable in the “**launch\_picontrol\_run\_global\_type**” file, set here at 360  
116 months (30 years).

117

118 2 Atmospheric regional model

119 2.1 Compiling the model

120 The code of this model is identical to that of the global version, but in “Makefile”, the key word  
121 should be changed from “lmdz96x71global” to “lmdz200120\_oneway”

122 Go to the following directory:

123 “**cd vadsaria\_et\_al\_model/LMDZ\_and\_NEMOMED8\_models/modipsl/config/LMDZ**”

124 Then compile the code through Makefile:

125 **gmake lmdz200120\_oneway**

126 where “**lmdz200120\_oneway**” is a keyword defined in the “**AA\_make**” script allowing a  
127 configuration to be chosen.

128 If the compilation is successful, executable files are stored in the following directory:

129 “**cd vadsaria\_et\_al\_model/LMDZ\_and\_NEMOMED8\_models/modipsl/modipsl/bin**”

130

131 2.2 Running the model

132 The first step is to create the boundary conditions for the regional atmospheric model. A boundary  
133 condition file, “**limit\_picontrol\_debiais.nc**”, is already provided in the following directory:

134 “**./vadsaria\_et\_al\_model/files\_and\_boundary\_conditions\_for\_LMDZ\_regional/start\_limit**”

135 It is of course different from that of the global model, but it is also obtained from the same bias-  
136 corrected SST and SIC data, derived from the IPSLCM5 global coupled model for the pre-industrial  
137 simulation. The procedure to generate this boundary condition file is the same as described for the  
138 global version.

139 To run the model, an example is given in the following directory

140 “**cd vadsaria\_et\_al\_model/files\_and\_boundary\_conditions\_for\_LMDZ\_regional**”

141 The example bash script “**launch\_picontrol\_run\_regional\_type**” shows how to run the atmospheric  
142 regional model. Unlike the global model, additional files are needed to nudge the regional model with  
143 the global output. “**biline\_poids\_s.nc**”, “**biline\_poids\_u.nc**” and “**biline\_poids\_v.nc**” (presented in  
144 the current directory) are interpolation files allowing efficient transformation of global variables for  
145 the regional model grid. Nudged forcing, with a 2-hour time step, from the global model is stored in  
146 “**sortie\_histfrq.nc**.”

147 Since the global and regional models share a common structure, their launch is also very similar,  
148 although with different configuration files.

149

150 3 Mediterranean oceanic model

151 NEMOMED8 is the Mediterranean regional version of the NEMO ocean modelling platform.

152 Documentation of the model can be found at: <http://forge.ipsl.jussieu.fr/nemo/wiki/Users>

153 3.1 Compiling the model

154 The compilation of NEMOMED8 is managed entirely through MODIPSL, so the generation of  
155 Makefile is the same as described earlier for LMDZ. The keyword to be used in the argument of  
156 “gmake” is “nemomed8”. The compilation procedure is simply the following:

157 **“cd vadsaria\_et\_al\_model/LMDZ\_and\_NEMOMED8\_models/modipsl/config/NEMOMED8”**

158 **“gmake nemomed8”**

159 **“cd vadsaria\_et\_al\_model/LMDZ\_and\_NEMOMED8\_models/modipsl/modipsl/bin”**

160 If the compilation is successful, then it creates the executable file, “opa”. In our study, NEMOMED8  
161 is compiled to run with 121 cores in parallel mode.

162 3.2 Running the model

163 Before running the model, the 3D boundary conditions for salinity and potential temperature over the  
164 buffer zone in the Atlantic close to the Gibraltar need to be generated. This operation is conducted in  
165 the following directory:

166 **“cd vadsaria\_et\_al\_model/files\_and\_boundary\_conditions\_for\_NEMOMED8”**

167 These boundary conditions are found in the files

168 **“data\_1m\_potential\_temperature\_nomask\_picontrol\_debiais\_climato.nc”** and

169 **“data\_1m\_salinity\_nomask\_picontrol\_debiais\_climato.nc”**, bias-corrected from the IPSLCM5 pre-  
170 industrial simulation. The grid of the NEMOMED8 model (**“meshmask\_med8.nc”**) is provided  
171 allowing the user to interpolate their own boundary conditions from this grid.

172 The second step is to generate the surface fluxes from the atmospheric regional model. For this  
173 purpose, an interpolation is used to convert the LMDZ4 air-sea fluxes into the NEMOMED8 grid  
174 (bilinear for wind stress and conservative remapping for other fluxes). For NEMOMED8, the water,  
175 radiative, latent, sensible fluxes and wind stress are required. In the sub-directory “/lmdz\_to\_nemo”, a  
176 code is provided to generate the bilinear interpolation scheme:

177 **“interpol\_between\_lmdz\_et\_nemo.F90”**. During the execution of the executable file, a weight file is  
178 required (**“opalmdmo”**, also provided in the sub-directory).

179 **“sst\_picontrol\_debiais.nc.000101”**,

180 **“flx\_picontrol\_debiais.nc.000101”**,

181 **“taux\_picontrol\_debiais.nc.000101”** and

182 **“tauy\_picontrol\_debiais.nc.000101”**.

183 Finally, the bash script **“launch\_picontrol\_run\_mediterranean\_ocean\_type”** is an example of the  
184 instructions necessary to run the oceanic regional model. The procedure is similar to the global and  
185 regional atmospheric model.

186

## 187 **Text S2: Bias correction**

188 The bias correction for our experiments driven by IPSL simulations is illustrated. IPSL-CM5A is a fully  
189 coupled climate system model. It operates autonomously for either present-day climate, future climate  
190 scenarios, or paleo climate reconstructions, depending on the external forcings or boundary conditions  
191 imposed on it. For its historical simulation of modern climate (from 1850 to 2005), we point out a few  
192 general biases that need to be corrected before running our regional system for paleo periods (Early  
193 Holocene). In the following, the bias-correction method for the oceanic 3-D structures, SST and SIC, as  
194 well as the freshwater discharges from rivers, is described.

195

### 196 *SST and SIC global fields*

197 The global fields of SST and SIC are the most important variables in our methodology since they contain  
198 the main climate change information to be transferred from global scale to regional scale. They are used  
199 to force both the AGCM and the ARCM. SST derived from IPSL-CM5A has a cold bias globally, which  
200 would exert strong impacts on the Mediterranean Sea and the nearby Atlantic region. To remove this  
201 bias, we simply applied an offset based on the difference between the IPSL-CM5A historical simulation  
202 and the ERA-Interim reanalysis (Dee et al., 2011) for the period 1970-1999.

203 IPSL-CM5A, on the other hand, tends to overestimate temperatures at the poles, which leads to an  
204 underestimation of the SIC. This bias affects the surface albedo and the global energy budget. It also  
205 affects the meridional temperature gradient and consequently the mid-latitude atmospheric eddies. The  
206 bias correction used for SIC is the analogue method presented in Beaumet et al. (2019). The basic idea  
207 is to adjust the total areas covered by sea ice for each hemisphere and for each month following the  
208 geographic and temporal biases. As with the previous corrections for SST, the hemispheric and monthly  
209 bias correction for SIC is based on the difference between IPSL simulations and observed SIC  
210 (Climatological monthly mean for 1970-1999 from ERA-Interim). Finally, the geographic distribution  
211 of SIC is determined by hemisphere and by month following an analogue relationship extracted to match  
212 observations from 1970 to 2012.

### 213 *3D temperatures and salinities in the buffer-zone*

214 The 3-D fields of oceanic temperature and salinity (over the whole water column) in the Atlantic buffer  
215 zone has been adjusted in the same way as for SST. We used the World Ocean Atlas (WOA) (Locarnini  
216 et al., 2013) as a reference to correct the outputs from the IPSL-CM5A historical simulation.

### 217 *River runoff to the Mediterranean Sea*

218 Freshwater discharge from rivers around the Mediterranean Sea is an important factor controlling the  
219 overturning circulation of the Mediterranean. Due to the high sensitivity of oceanic circulation to this  
220 variable, we decided to apply a bias-correction to calibrate the river discharges produced by LMDZ-  
221 regional. Actually, the atmospheric model, coupled to the land surface model ORCHIDEE, tends to  
222 overestimate the amount of freshwater runoffs compared to present-day observations (Figure S1). The  
223 bias-corrected that we applied is based on the observed climatological runoff (Ludwig et al. 2009;  
224 Vorosmarty et al., 1998) and the differences between the Early Holocene simulation and present-day  
225 simulation. When the difference is relatively not significant, the corrected runoff is set to the  
226 climatology, mainly to avoid negative values<sup>1</sup>. However, in order to stay consistent with the  
227 methodology for SST and SIC bias correction, we chose the absolute difference correction method for  
228 the river runoff.

229

### 230 **Text S3: Comparison of model simulation outputs and reconstructed data for the Mediterranean** 231 **basin**

#### 232 *Continental precipitation*

233 The reconstructed data used for comparison with the EHOL simulation is taken from Dormoy et al.  
234 (2009) for the Aegean Sea, from Peyron et al. (2011) for the Lake Accesa and Tenaghi Philippon, and  
235 Magny et al. (2013) for Lake Pergusa. In these studies, continental precipitation is reconstructed based  
236 on pollen sequences to emphasize the changes in precipitation seasonality. Several methods are used to  
237 determine these changes. We chose to reconstruct these changes using the Modern Analogue Technique  
238 (MAT, Guiot, 1990), because, in their study, Magny et al. (2013) compared their data to Peyron et al.  
239 (2011). We extracted data values framing a few hundred years around 9.5 ka cal BP, consistent with  
240 the orbital parameters of our atmospheric simulations (both global and regional). For the Northern  
241 Sahara, data are based on  $\delta^{18}\text{O}$  from Bar-Matthews et al. (2003).

242 Comparison between model outputs and reconstruction data in terms of annual and seasonality changes  
243 can be conducted and anomalies against modern values can be shown. In winter, the model shows  
244 positive precipitation anomalies for the four sites (Lake Accesa, model: 20-36 mm, data: 20-40mm,  
245 Tenaghi Philippon, model: 30-45 mm, data: 10-35 mm, Aegean, model: 29-45 mm, data: 10-80mm,  
246 Lake Pergusa, model: 7-26 mm, data: 35-60mm, Table S1). In summer, the model shows a more  
247 contrasted response, with negative anomalies in summer temperatures (Table S1) due to the homogenous  
248 drought (Fig 10d in the main article). However, this comparison cannot reflect the precipitation changes  
249 for the entire continent. Indeed, in north of Lake Accesa we see positive summer anomalies (Fig 10d in  
250 the main article).

---

<sup>1</sup> Namely, when the difference does not exceed 25%, of the annually average annual difference for the Nile river runoff (due to the simulated amplitude, cf section 4.4) and 5% for the rest of the rivers.



251

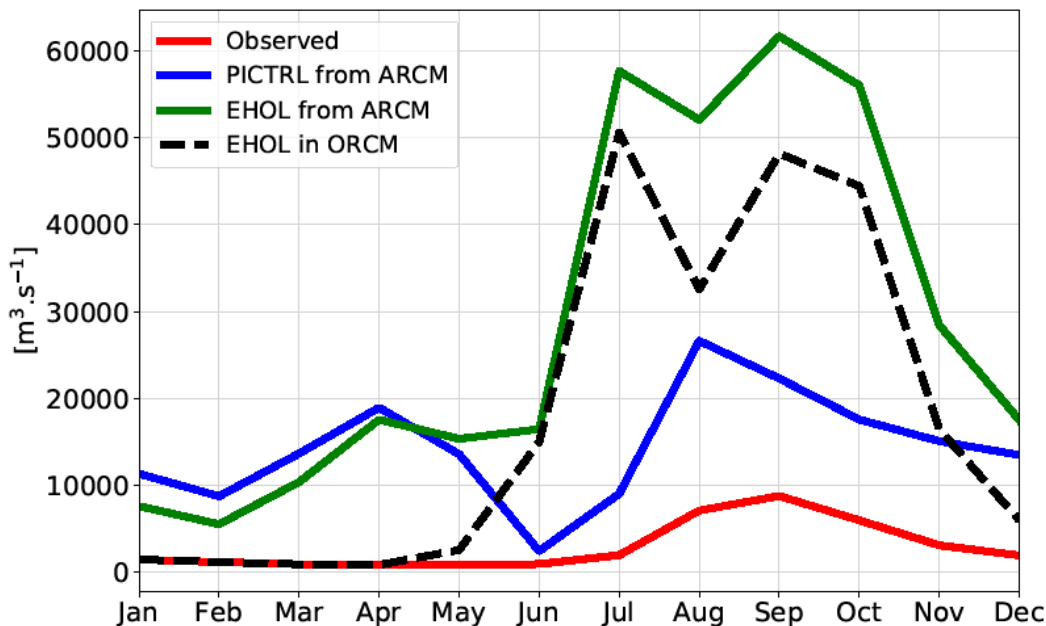
## 252 *Sea Surface Temperatures*

253 We conducted a comparison of model output and data for SST as Adloff et al., (2011) did with the  
254 reconstruction of Kucera et al., (2011) (unpublished work). This reconstruction is based on census  
255 counts of foraminiferal species, and on the artificial neural network for the transfer function. The data  
256 used span the Holocene Insolation maximum interval (8.5 - 9.5 ka BP). Winter SST values (January to  
257 March, Figure S2, f) are a bit lower than the reconstruction especially for the Eastern basin (-1 to -2 °C).  
258 The simulated summer SSTs (July to September, Figure S3, j) are higher between the Tyrrhenian Sea  
259 and the Levantine Sea (+1 to +4 °C). This enhanced contrast between winter and summer values for  
260 simulated SST produced an annual signal in good agreement with the reconstructed values (Figure S3,  
261 c). Our results depict the same signal pattern as the simulations of Adloff et al. (2011) do, with some  
262 differences in the enhanced seasonal contrast. In Figure S3 are also depicted the same climatology for  
263 the bias Early Holocene SST and the bias corrected Early Holocene SST boundary conditions used in  
264 the model architecture. This figure shows how the SST signal have been improved, from the bias  
265 correction to the ORCM simulation, in order to range the reconstruction with the use of the regional  
266 models.

267

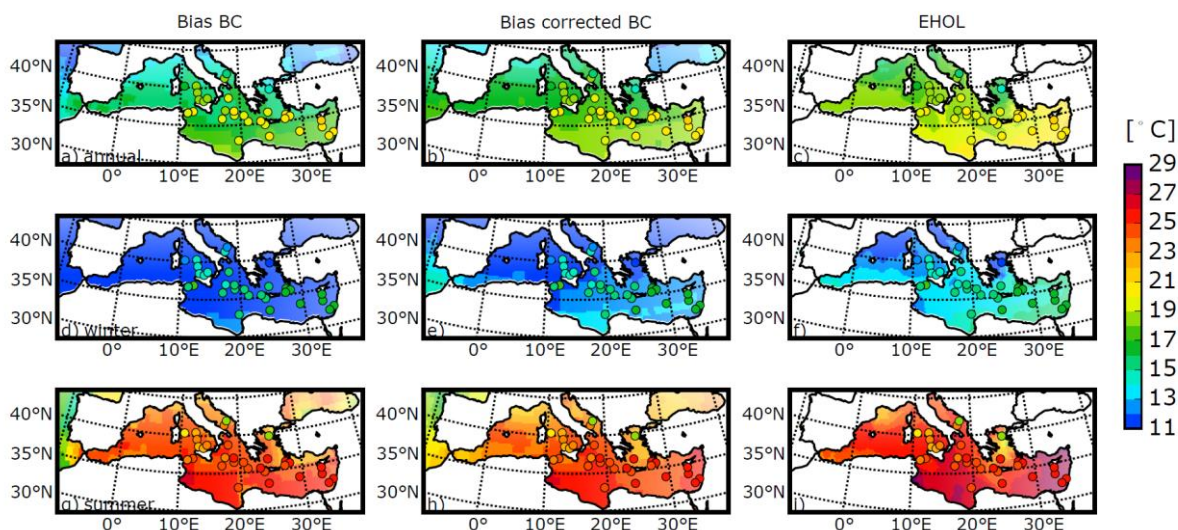
## 268 *Sea Surface Salinities*

269 The comparison of SSS over the Mediterranean Sea provides an appropriate indicator of freshwater  
270 perturbation induced by enhanced river fluxes. As a reference for comparison, we use a synthesis of SSS  
271 sampled from the S1 deposition, and provided by Kallel et al. (1997). Our EHOL simulation takes the  
272 Nile river enhancement into account, that is an annual river discharge of  $13000 \text{ m}^3 \cdot \text{s}^{-1}$ , against  $2930 \text{ m}^3 \cdot \text{s}^{-1}$   
273 <sup>1</sup> for the pre-industrial value). The North-East rivers (Buyukmenderes, Vardar, Acheloos, Vjosa,  
274 Semanit, Shkumbin, Durres, Mat and Drini) have their annual fresh water discharges increasing from  
275  $1082 \text{ m}^3 \cdot \text{s}^{-1}$  at pre-industrial level to  $1622 \text{ m}^3 \cdot \text{s}^{-1}$ . The fresh water discharge from February to May  
276 increases even more, from  $1619 \text{ m}^3 \cdot \text{s}^{-1}$  at pre-industrial level to  $3228 \text{ m}^3 \cdot \text{s}^{-1}$  for EHOL. Our EHOL  
277 simulation, even with a significant increase of freshwater inputs, still cannot reproduce a sufficient  
278 decrease of SSS to match the reconstructed values, as shown in Figure S3. . Rohling (1999, 2000)  
279 pointed out that this mismatch can be partly attributed to uncertainties in salinity reconstruction. It is not  
280 always straightforward to interpret the isotopic composition of oxygen in terms of salinity. Finally, it is  
281 likely that an additional non-negligible fresh water source is missing. To explain the substantial SSS  
282 decrease, an additional source of freshwater associated with an amplification of the flux of the North  
283 African rivers could potentially be superimposed on the Nile. Indeed, changes of this type in the  
284 hydrology are clearly indicated by the data but are not reproduced in most of the Early and Mid-  
285 Holocene simulations.



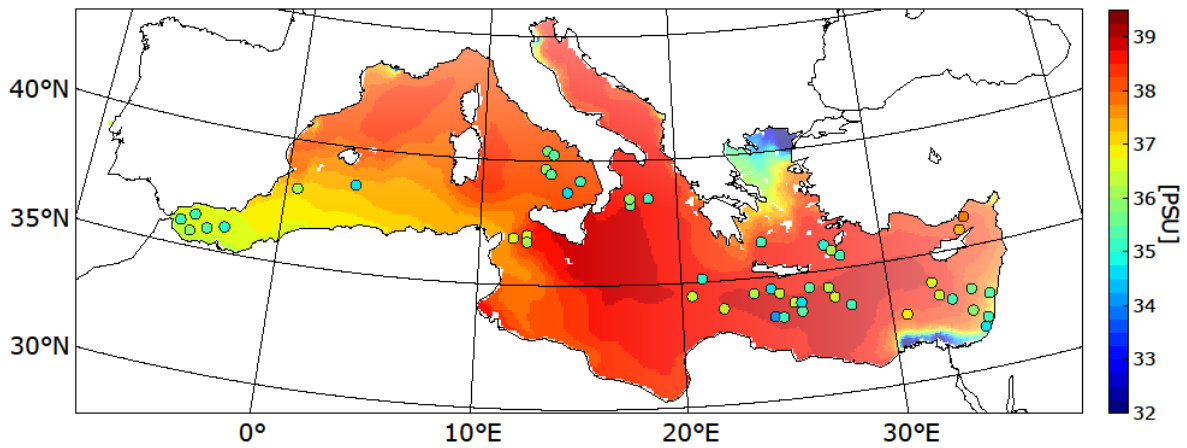
287  
 288 **Figure S1: climatological runoff of the Nile River, observed pre-damming values (red), runoff as**  
 289 **simulated by the ARCM, PICTRL (blue) and EHOL (green), and corrected runoff used in the**  
 290 **ORCM.**

291  
 292

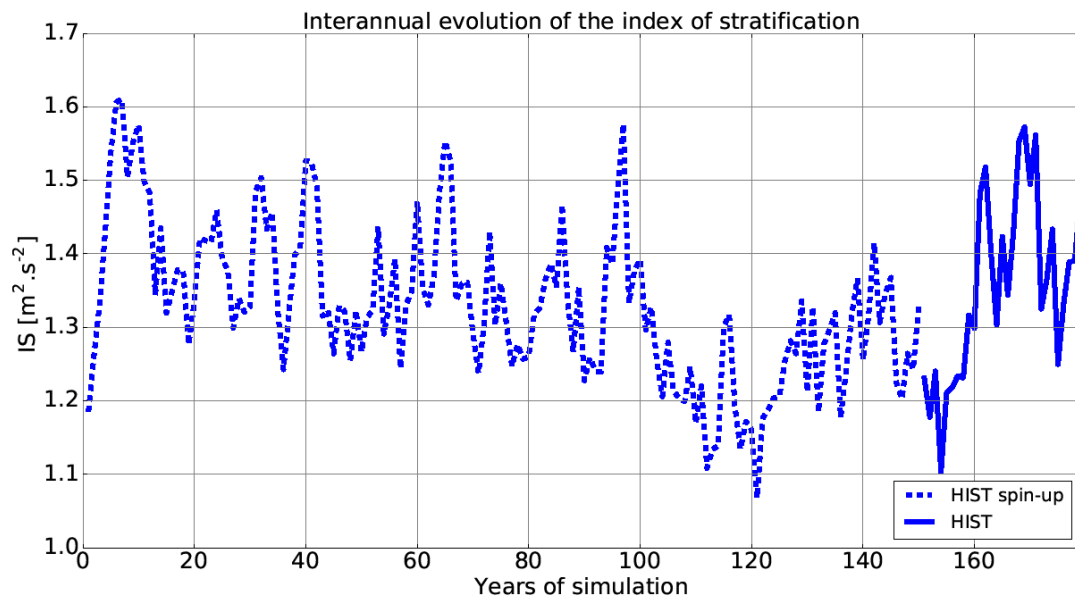


293  
 294  
 295 **Figure S2: Model-data comparison for SST, adapted from Adloff (2011). Dots represent the**  
 296 **unpublished synthesis of Kucera et al. (2011), published in Adloff (2011). The background colour**  
 297 **represents, in the first column, the bias SST boundary conditions (BC) derived from the Early**

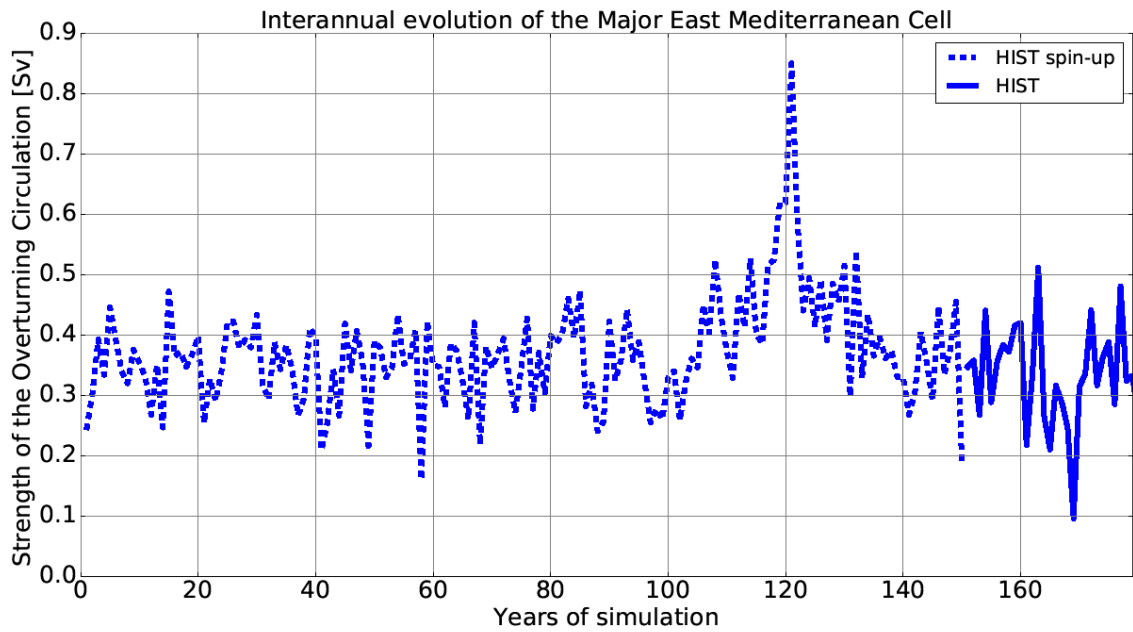
298 **Holocene IPSL-CM5 simulation (AMIP resolution), in the second column, the bias corrected SST**  
 299 **BC as it has been used to drive the AGCM and the AGCM both (AMIP resolution), and, in the**  
 300 **third column, SST in the EHOL experiment realized with the ORCM (1/8°, averaged over the last**  
 301 **30 years of simulation).**  
 302



303  
 304 **Figure S3: Model-data comparison for SSS. Dots represent the synthesis of Kallel et al. (1997a).**  
 305 **The background colour represents the EHOL simulation.**  
 306

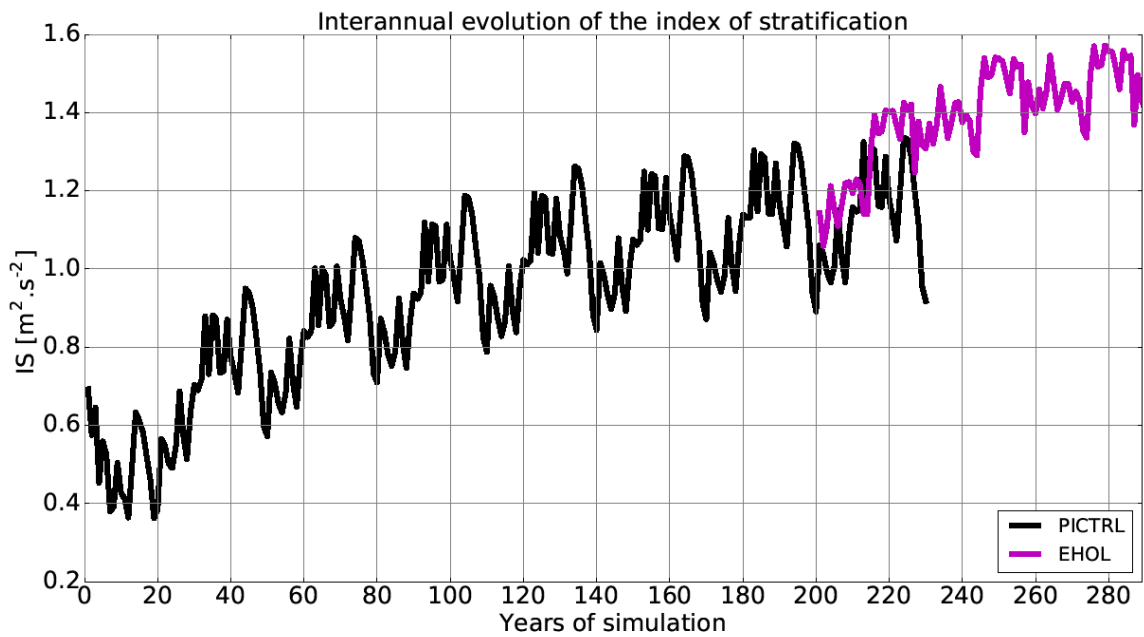


307  
 308 **Figure S4: Interannual evolution of the index of stratification (IS) for the Mediterranean Sea for**  
 309 **the HIST simulation (including the spin-up phase).**



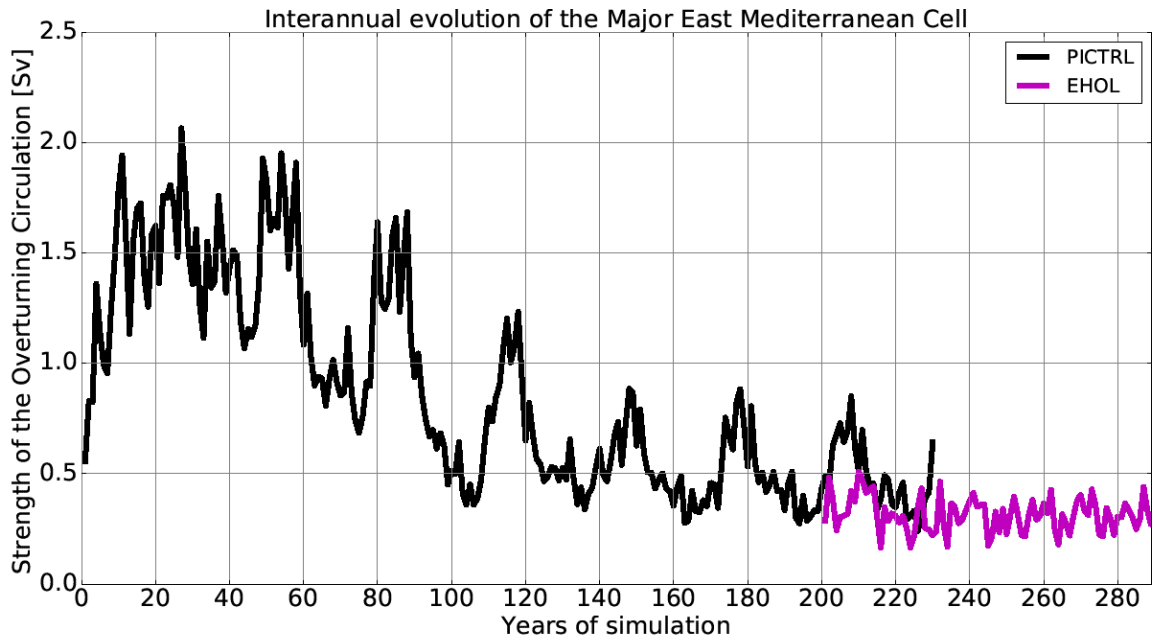
310

311 **Figure S5: Interannual evolution of the Zonal overturning Stream Function (ZOF) in the eastern**  
 312 **Mediterranean Sea for the HIST simulation (including the spin-up phase).**



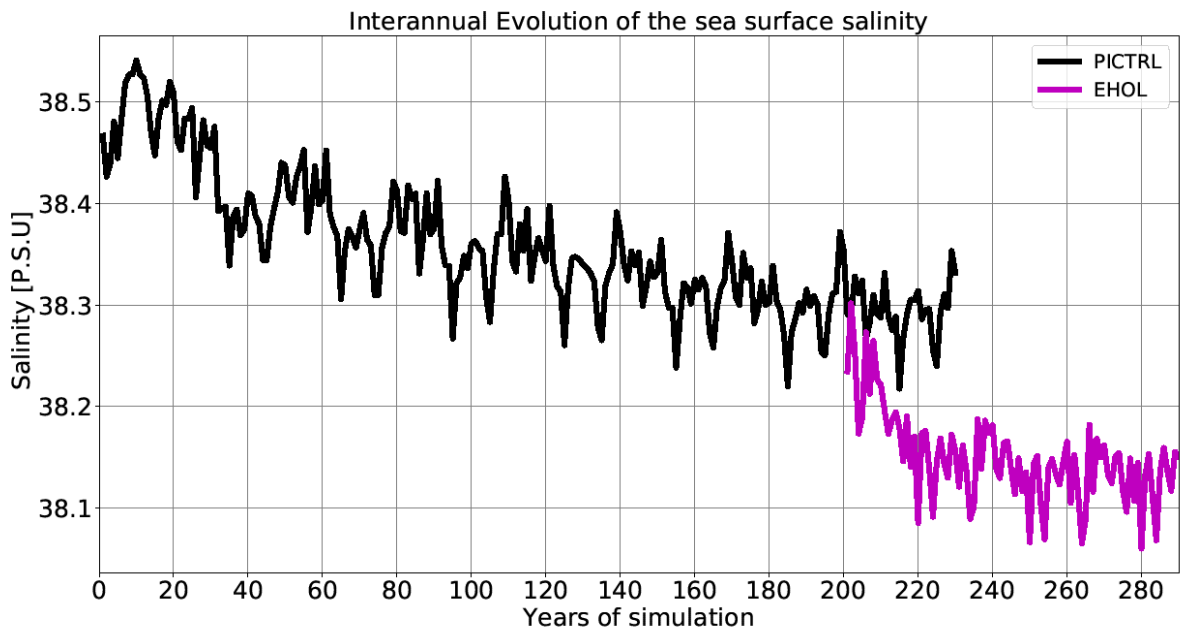
313

314 **Figure S6: Interannual evolution of the index of stratification (IS) for the Mediterranean Sea for**  
 315 **the PICTRL and EHOL simulations (including the PICTRL spin-up phase).**



316

317 **Figure S7: Interannual evolution of the Zonal overturning Stream Function (ZOF) in the eastern**  
 318 **Mediterranean Sea for the PICTRL and EHOL simulations (including the PICTRL spin-up**  
 319 **phase).**



320

321 **Figure S8: Interannual evolution of the sea surface salinity (SSS) for the Mediterranean Sea for**  
 322 **the PICTRL and EHOL simulations (including the PICTRL spin-up phase).**

323

324

Precipitation (mm)	Winter			Summer			Annual		
	MODERN	$\Delta$ OBS	$\Delta$ EHOL	MODERN	$\Delta$ OBS	$\Delta$ EHOL	MODERN	$\Delta$ OBS	$\Delta$ EHOL
Lake ACESSA	240	20-40	20-36	80	0-30	(-26)-(-8)	750	10-70	8-60
Tenaghi Philippon	225	10-35	30-45	80	20-50	(-13)-5	600	130-225	17-49
Lake Pergusa	225	35-60	7-26	80	30-50	(-17)-(-3)			
Aegean Sea	200	10-80	29-45	40	0-40	(-19)-0			
Northern Sahara							<200	700-800	(-20)-15

325

326 **Table S1: Model-data comparison for continental. First row: Lake ACESSA (Northern Italy)**  
327 **(Peyron et al., 2011), Second row: Tenaghi Philippon, (Greece) (Peyron et al., 2011), Third row:**  
328 **Lake Pergusa (Sicily), (Magny et al., 2013), Fourth row: Aegean Sea, (Dormoy et al., 2009), Fifth**  
329 **row: Northern Sahara (Bar-Matthews et al., 2003). “MODERN” refers to the present values of**  
330 **precipitation, “OBS” to the data (around 9.5 ka cal BP), and “EHOL” for the Early Holocene**  
331 **simulation described in the article.**

332

333

	HIST	PICTRL	EHOL
Orbital parameters	$e = 0.01672$ $\varepsilon = 23.44$ $\omega -180 = 102.7$	Same as in HIST	$e = 0.01935$ $\varepsilon = 24.231$ $\omega -180 = 303.3$
Atmospheric CO <sub>2</sub>	Annual observed global mean (1970-1999)	284 ppm	284 ppm
SST forcing	Era-Interim monthly forcing (1970-1999)	IPSL-CM5A picontrol + SST correction	IPSL-CM5A early Holocene + SST correction
SIC forcing	Era-Interim monthly forcing (1970-1999)	IPSL-CM5A picontrol + SIC correction	IPSL-CM5A Early Holocene + SIC correction

334

335 **Table S2: Forcings and parameters used in both AGCM and ARCM.  $\varepsilon$  is the elliptic orbit**  
336 **obliquity,  $e$ , the eccentricity and  $\omega$ , the longitude of the perihelion. The reader can notice that the**

337 **pCO<sub>2</sub> should be 260 ppm as suggested by the PMIP protocol for mid-Holocene. The goal in this**  
 338 **paper was mainly to have a sensitivity to orbital parameters.**

339

340

	HIST	PICTRL	EHOL
Buffer-zone T3D & S3D	WOA monthly forcing (1970-1999 mean)	IPSL-CM5A picontrol + T3D/S3D correction	IPSL-CM5A early Holocene + T3D/S3D correction
River runoff	Ludwig et al 2009, Rivdis database	Ludwig et al 2009, Rivdis database (But Pre-damming Nile)	Anomalies inferred from EHOL – PICTRL atmospheric simulations (NILE + East-North margin)

341

342 **Table S3: Forcings used in the ORCM.**

343

#### 344 **References**

345 Adloff, F., Mikolajewicz, U., Kučera, M., Grimm, R., Maier-Reimer, E., Schmiedl, G. and Emeis, K.  
 346 C.: Upper ocean climate of the Eastern Mediterranean Sea during the Holocene Insolation Maximum -  
 347 A model study, *Clim. Past*, 7(4), 1103–1122, doi:10.5194/cp-7-1103-2011, 2011.

348 Bar-Matthews, M., Ayalon, A., Gilmour, M., Matthews, A. and Hawkesworth, C. J.: Sea - land oxygen  
 349 isotopic relationships from planktonic foraminifera and speleothems in the Eastern Mediterranean  
 350 region and their implication for paleorainfall during interglacial intervals, *Geochim. Cosmochim. Acta*,  
 351 67(17), 3181–3199, doi:10.1016/S0016-7037(02)01031-1, 2003.

352 Beaumet, J., Krinner, G., Déqué, M., Haarsma, R. and Li, L.: Assessing bias-corrections of oceanic  
 353 surface conditions for atmospheric models, *Geosci. Model Dev. Discuss.*, (December), 1–29,  
 354 doi:10.5194/gmd-2017-247, 2017.

355 Dee, D. P., Uppala, S. M., Simmons, A. J., Berrisford, P., Poli, P., Kobayashi, S., Andrae, U.,  
 356 Balmaseda, M. A., Balsamo, G., Bauer, P., Bechtold, P., Beljaars, A. C. M., van de Berg, L., Bidlot, J.,  
 357 Bormann, N., Delsol, C., Dragani, R., Fuentes, M., Geer, A. J., Haimberger, L., Healy, S. B., Hersbach,  
 358 H., Hólm, E. V., Isaksen, L., Kållberg, P., Köhler, M., Matricardi, M., McNally, A. P., Monge-Sanz, B.

359 M., Morcrette, J. J., Park, B. K., Peubey, C., de Rosnay, P., Tavolato, C., Thépaut, J. N. and Vitart, F.:  
360 The ERA-Interim reanalysis: Configuration and performance of the data assimilation system, *Q. J. R.*  
361 *Meteorol. Soc.*, 137(656), 553–597, doi:10.1002/qj.828, 2011.

362 Dormoy, I., Peyron, O., Combourieu Nebout, N., Goring, S., Kotthoff, U., Magny, M. and Pross, J.:  
363 Terrestrial climate variability and seasonality changes in the Mediterranean region between 15 000 and  
364 4000 years BP deduced from marine pollen records, *Clim. Past*, 5, 615–632, 2009.

365 Guiot, J.: Methodology of the last climatic cycle reconstruction in France from pollen data, *Palaeogeogr.*  
366 *Palaeoclimatol. Palaeoecol.*, 80(1), 49–69, doi:10.1016/0031-0182(90)90033-4, 1990.

367 Kallel, N., Paterne, M., Labeyrie, L., Duplessy, J. C. and Arnold, M.: Temperature and salinity records  
368 of the Tyrrhenian Sea during the last 18,000 years, *Palaeogeogr. Palaeoclimatol. Palaeoecol.*, 135(1–4),  
369 97–108, doi:10.1016/S0031-0182(97)00021-7, 1997.

370 Kucera, M., Rohling, E. J., Hayes, A., Hopper, L. G. S., Kallel, N., Buongiorno Nardelli, B., Adloff, F.  
371 and Mikolajewicz, U.: Sea surface temperature of the Mediterranean Sea during the early Holocene  
372 insolation maximum, *Clim. Past*, 2011.

373 Locarnini, R. A., Mishonov, A. V., Antonov, J. I., Boyer, T. P., Garcia, H. E., Baranova, O. K., Zweng,  
374 M. M., Paver, C. R., Reagan, J. R., Johnson, D. R., Hamilton, M. and Seidov, D.: *World Ocean Atlas*  
375 2013, Volume 1: Temperature, NOAA Atlas., edited by S. Levitus and A. Mishonov., 2013.

376 Ludwig, W., Dumont, E., Meybeck, M. and Heussner, S.: River discharges of water and nutrients to the  
377 Mediterranean and Black Sea: Major drivers for ecosystem changes during past and future decades?,  
378 *Prog. Oceanogr.*, 80(3–4), 199–217, doi:10.1016/j.pocean.2009.02.001, 2009.

379 Magny, M., Combourieu-Nebout, N., De Beaulieu, J. L., Bout-Roumazeilles, V., Colombaroli, D.,  
380 Desprat, S., Francke, A., Joannin, S., Ortu, E., Peyron, O., Revel, M., Sadori, L., Siani, G., Sicre, M. A.,  
381 Samartin, S., Simonneau, A., Tinner, W., Vanni re, B., Wagner, B., Zanchetta, G., Anselmetti, F.,  
382 Brugiapaglia, E., Chapron, E., Debret, M., Desmet, M., Didier, J., Essallami, L., Galop, D., Gilli, A.,  
383 Haas, J. N., Kallel, N., Millet, L., Stock, A., Turon, J. L. and Wirth, S.: North-south palaeohydrological  
384 contrasts in the central mediterranean during the holocene: Tentative synthesis and working hypotheses,  
385 *Clim. Past*, 9(5), 2043–2071, doi:10.5194/cp-9-2043-2013, 2013.

386 Peyron, O., Goring, S., Dormoy, I., Kotthoff, U., Pross, J., de Beaulieu, J.-L., Drescher-Schneider, R.,  
387 Vanni re, B. and Magny, M.: Holocene seasonality changes in the central Mediterranean region  
388 reconstructed from the pollen sequences of Lake Accessa (Italy) and Tenaghi Philippon (Greece), *The*  
389 *Holocene*, 21(1), 131–146, doi:10.1177/0959683610384162, 2011.

390 Rohling, E. J.: Environmental control on Mediterranean salinity and  $\delta^{18}\text{O}$ , *Paleoceanography*, 14(6),  
391 706–715, doi:10.1029/1999PA900042, 1999.



392 Rohling, E. J.: Paleosalinity: Confidence limits and future applications, *Mar. Geol.*, 163, 1–11,  
393 doi:10.1016/S0025-3227(99)00097-3, 2000.

394 Vadsaria, T., Li, L., Ramstein, G., & Dutay, J.-C.: Model and output for Vadsaria et al, “Development  
395 of a sequential tool LMDZ-NEMO-med-V1 for global to regional past climate simulation over the  
396 Mediterranean basin: an early Holocene case study”, GMD publication. doi:[10.5281/zenodo.3258409](https://doi.org/10.5281/zenodo.3258409),  
397 2019.

398 Vorosmarty, C. J., Feteke, B. M. and Tucker, B. A.: *Global River Discharge, 1807-1991*, V. 1.1  
399 (RivDIS), 1998.

400